Biochemical and Biophysical Research Communications 450 (2014) 1684–1689

Contents lists available at ScienceDirect

Biochemical and Biophysical Research Communications

journal homepage: www.elsevier.com/locate/ybbrc

Non-destructive observation of intact bacteria and viruses in water by the highly sensitive frequency transmission electric-field method based on SEM

Toshihiko Ogura

Biomedical Research Institute, National Institute of Advanced Industrial Science and Technology (AIST), Central 2, Umezono, Tsukuba, Ibaraki 305-8568, Japan

ARTICLE INFO

Article history:
Received 4 July 2014
Available online 21 July 2014

Keywords:
Scanning electron microscopy
Beam blanking
Wet biological specimen
Silicon nitride film
Bias voltage

ABSTRACT

The high-resolution structural analysis of biological specimens by scanning electron microscopy (SEM) presents several advantages. Until now, wet bacterial specimens have been examined using atmospheric sample holders. However, images of unstained specimens in water using these holders exhibit very poor contrast and heavy radiation damage. Recently, we developed the frequency transmission electric-field (FTE) method, which facilitates the SEM observation of biological specimens in water without radiation damage. However, the signal detection system presents low sensitivity. Therefore, a high EB current is required to generate clear images, and thus reducing spatial resolution and inducing thermal damage to the samples. Here a high-sensitivity detection system is developed for the FTE method, which enhances the output signal amplitude by hundredfold. The detection signal was highly enhanced when voltage was applied to the metal layer on silicon nitride thin film. This enhancement reduced the EB current and improved the spatial resolution as well as the signal-to-noise ratio. The spatial resolution of a high-sensitive FTE system is 41 nm, which is considerably higher than previous FTE system. New FTE system can easily be utilised to examine various unstained biological specimens in water, such as living bacteria and viruses.

1. Introduction

High-resolution imaging of biological specimens by electron microscopy provides valuable insight to biological mechanisms [1–6]. In particular, scanning electron microscopy (SEM) has widely been used to analyse bacterial and viral structures [7–12]. However, SEM observations of these specimens under high vacuum conditions require specific sample preparation protocols involving glutaraldehyde fixation, negative staining, cryo-techniques and metal coating or labelling to avoid electrical radiation damage [10–13]. These protocols also enhance contrast and prevent the electrical charging of the specimens. Until now, atmospheric and/or wet biological specimens have been examined using atmospheric holders [14,15], but they undergo heavy radiation damage caused by electron beam (EB) [16–18]. In addition, images of unstained samples display very poor contrast. Therefore, these systems require additional glutaraldehyde fixation with negative staining or metal labelling [14,15].

The SEM-based frequency transmission electric-field (FTE) method has recently been developed for the non-destructive analysis of biological specimens in water [19]. In this FTE system, we combined both technologies of the electrical impedance tomography method [20–24] and the ultrasonic imaging method based on SEM [25,26]. Our FTE method provides high-contrast imaging of the intact specimens in water introduced in an atmospheric sample holder comprising two silicon nitride (SiN) films [19]. The upper SiN film, which is coated with tungsten–nickel (W–Ni), is irradiated using a focused modulation EB. Irradiated electrons are strongly scattered and absorbed in the 20 nm-thick W layer resulting in a negative electric-field potential at the irradiated position. This negative potential oscillates at the EB modulation frequency (30–60 kHz) and is transmitted to the bottom SiN film through the biological sample. In this method, the biological samples are not directly exposed to the EB, which prevents electron radiation damage [19]. However, the signal detection system presents low sensitivity. Therefore, a high EB current is required to generate clear images, and thus reducing spatial resolution and inducing thermal damage to the samples.

Here, a highly sensitive detection system is presented for the FTE method to enhance the output signal amplitude (Fig. 1). This

E-mail address: t-ogura@aist.go.jp

http://dx.doi.org/10.1016/j.bbrc.2014.07.062
0006-291X/

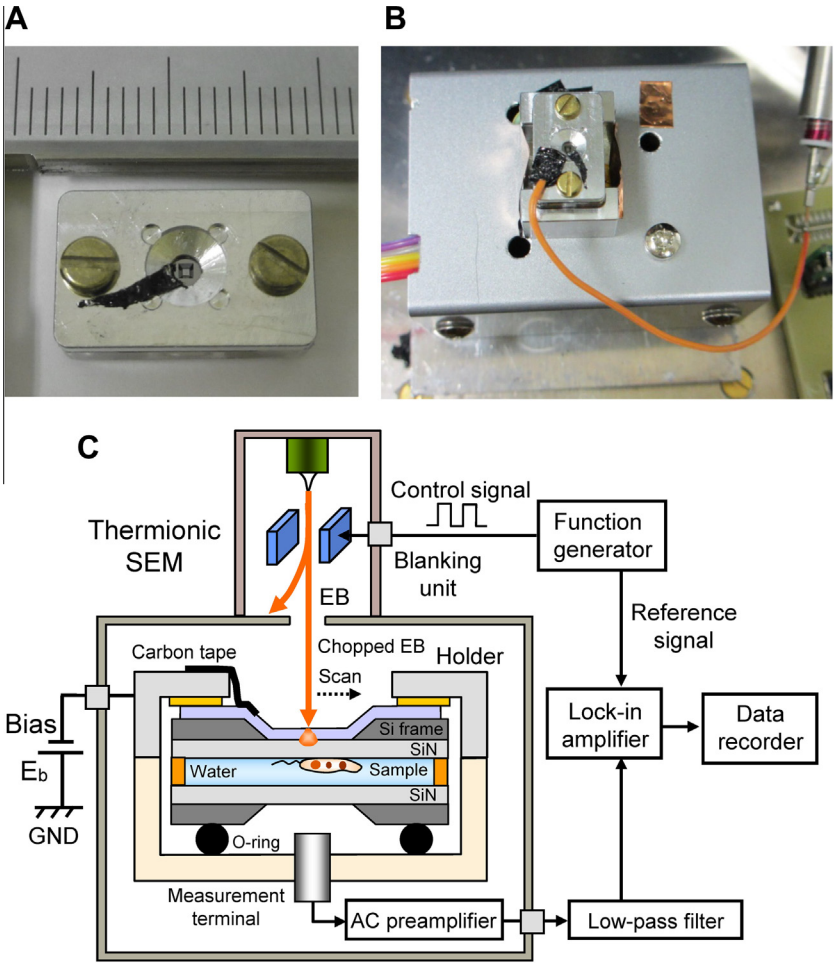

Fig. 1. Experimental set-up and the highly sensitive SEM-based FTE imaging system. (A) Photograph of a sample holder. The sample space between the SiN films was sealed using double-sided tape and two screws. The W–Ni layer was connected to the upper Al holder part using conductive carbon tape. (B) Photograph of a water sample holder set on the AC pre-amplifier box. The sample holder was mounted on the Al stage. To apply bias, a cable connected the upper Al holder part to the bias voltage source (Model 6430, Keithley). (C) Schematic diagram of the electrically biased FTE system. Biological specimens in water were introduced in the 5 μm-thick space between two SiN films. The scanning EB, which was modulated by a beam blanking unit using a function generator at 30 kHz, irradiated the W–Ni coated SiN film at a 4 kV acceleration voltage. The measurement terminal under the holder detected the frequency signal from the W–Ni layer through the specimens. The output signal from the lock-in amplifier was recorded by a data recorder. The bias voltage was applied to the W–Ni layer.

enhancement is expected to considerably reduce the EB current; therefore, improving spatial resolution and signal-to-noise ratio (SNR). This approach offers a high-resolution and clear observation of unstained bacteria and viruses in water.

2. Materials and methods

2.1. Metal deposition on the upper SiN film

A 50 nm-thick SiN film supported by a 0.4 × 0.4 mm window in a Si frame (4 × 4 mm, 0.38 mm thickness, Silson Ltd., UK) was successively coated with W and Ni using a magnetron sputtering machine (Model MSP-30T, Vacuum Device Inc., Japan). As previously described [19], nickel sputtering was conducted for 5 s under 1.1 Pa Ar at 200 mA to generate a 5 nm-thick layer. Tungsten was sputtered for 20 s at 1.1 Pa Ar and 200 mA giving a 20 nm-thick coat. The distance between the sputter target and SiN film amounted to 50 mm.

2.2. Sample preparation

The purple, rod-shaped, non-sulphur photosynthetic bacterium bearing flagella *Rhodobacter capsulatus* [27–29] was obtained from the Santechno Co. (Japan, Osaka). The bacterial solution (1 ml) was centrifuged at 6,200 rpm for 1 min using a Capsulefuge PMC-060 (Tomy Inc., Japan) and the supernatant solution was replaced by 0.5 ml solution of 1% (w/v) trehalose (Hayashibara Inc., Japan) and 0.5% NaCl. The sample solution (2 μl) was introduced in the atmospheric holder.

The *Spodoptera litura* nuclear polyhedrosis virus (SNPV) was provided by Nippon Kayaku Co. Ltd. (Japan). The SNPV powder (10 mg) was dissolved in 20 mM sodium carbonate solution (pH 11.0, 1 ml) for 10 min and the baculovirus solution (2 μl) was introduced in the holder.

2.3. Atmospheric sample holder

A holder consisting of an upper aluminium (Al) part and a lower acrylic resin part maintained the sample solution at atmospheric pressure between the SiN films (Fig. 1). The upper W–Ni-coated SiN film was attached by a 5 μm-thick double-sided tape (No. 5600, Nitto Denko Co., Japan). The holder parts were fixed with double-sided tape (No. 7602, Teraoka Seisakusho Co., Ltd., Japan) and screwed together to seal the two SiN films containing the liquid sample (Fig. 1A). To allow conduction to the W–Ni layer, the Al holder part was connected to a sub-femtoamp remote

source metre supplying a voltage bias (Model 6430, Keithley Instruments Inc., USA) using a conductive carbon tape including Al thin film (#15-1097, OkenShoji Co., Japan). The resin holder part displayed high resistivity, insulating the terminal underside of the holder from the metal-coated SiN film (Fig. 1B).

2.4. SEM and high-sensitivity FTE system

The high-sensitivity SEM-based FTE imaging setup is illustrated in Fig. 1C. A beam blanking unit (Sanyu Electron Co., Japan) consisting of deflection plates was introduced into a thermionic emission JSM-6390 instrument (JEOL, Japan). The blanking unit was controlled by a function generator (WF1974, NF Co., Japan) using a square wave at a frequency of 30 kHz and voltage intensities of 0–10 V [19]. The atmospheric sample holder was mounted onto an Al stage over the W–Ni-coated SiN film and the measurement terminal was connected to an alternating current (AC) preamplifier, exhibiting a cut-off frequency of 1 kHz and an amplitude magnification of 1000×. The electric frequency signal from the preamplifier was entered into the lock-in amplifier (LI5640, NF Co., Japan) after the low-pass filter (cut-off frequency 150 kHz) (Fig. 1C). The lock-in amplifier was set as AC signal input and 24 dB filter and 100-μs outputs. The lock-in amplifier output and XY scanning signal were logged at a sampling frequency of 20 kHz using the data recorder (EZ7510, NF Co., Japan). SEM images (1280 × 960 pixels) were captured at a magnification of 2000–10,000× scanning time of 160 s, working distance of 7 mm, EB acceleration voltage of 4 kV and current of 200−2400 pA.

2.5. Image processing

Recorded FTE-signal data files were transferred to a personal computer (Intel Core i7, 2.8 GHz, Windows 7), and FTE images were processed using the Matlab R2007b software with an image processing toolbox (Math Works Inc., USA). Original FTE images were filtered using a two-dimensional (2D) Gaussian filter (GF) with kernel sizes of 7 × 7 pixels and 11 × 11 pixels ($1-3\sigma$). Background subtraction was performed by subtracting FTE images from filtered images at broad GF (201 × 201 pixels, 80σ). The SNR is calculated by the ratio of the image signal (S_i) to the mean square error (N_{mse}) of background noise (Eq. (1)).

$$\mathrm{SNR} = 10\log_{10}\frac{S_i^2}{N_{mse}} \tag{1}$$

Here, S_i is a signal range of the broad GF filtered image (61 × 61 pixels, 30σ), which is obtained from subtraction of its image maximum value and a minimum value.

3. Results

Unstained and unfixed biological specimens in water that were introduced in the sample holder comprised of metal-coated and uncoated SiN films (Fig. 1A). The upper aluminium holder part was connected to the electric bias supply positioned outside the SEM instrument via conductive carbon tape (Fig. 1A and B). Consequently, the voltage of the W–Ni layer was controlled by the bias supply. The acrylic resin holder part presented high resistivity, insulating the measurement terminal from the metal-coated SiN film. This prevented the direct detection of the EB signal through the W–Ni layer.

The high-sensitivity SEM-based FTE imaging method is illustrated in Fig. 1C. In this method, a beam blanking unit installed in a thermionic SEM instrument served as an electrostatic deflection system [19]. A 30 kHz square wave used as a control signal was applied to the deflection plate to produce the focused modulation EB. The W–Ni-coated SiN film on the sample holder was irradiated using the resulting chopped EB at a low acceleration voltage of 4 kV. A measurement terminal under the sample holder detected the electric frequency signal of the EB-irradiated position through the biological specimens [19]. This signal underwent AC pre-amplification through a low-pass filter before entering a lock-in amplifier that generated the final output (Fig. 1C). Finally, output and EB scanning signals from the data recorder provided the FTE images.

To investigate output amplitudes in water, the lock-in-amplifier output was measured at various bias voltages (Supplementary Fig. 1). The output amplitude exhibited a maximum value of 150 mV at a bias voltage of −30 V. This amplitude decreased linearly when the bias voltage increased from −30 to 0 V. A bias of 0 V resulted in a signal output of 1.5 mV, which is approximately one hundredfold lower than at −30 V bias voltage. The output amplitude rose to 80 mV when the bias voltage continuously increased from 0 to +30 V. However, this amplitude is approximately half of that obtained at −30 V bias voltage (Supplementary Fig. 1). In the previous FTE system, the bias voltage of the metal layer was connected to the system ground (GND), which corresponds to a bias voltage of 0 V [19], minimising the output signal amplitude and limiting detection. In contrast, the newly developed FTE system enhanced the output signal by hundredfold at a bias voltage of −30 V.

Next, unstained and unfixed *Rhodobacter capsulatus* [27–29] was examined in water and air (Supplementary Fig. 2). In water, these rod-shaped bacteria exhibited weak black contrast at a bias of −30 V (Supplementary Fig. 2A). The contrast between background and bacterial contour displayed slight undulation, reflecting water thickness. The black contrast was enhanced in air (Supplementary Fig. 2B). Furthermore, the undulation contrast around the bacteria was flat in air. Therefore, bacteria in water may be distinguished from those in air using image contrast.

To investigate bacterial contrast in water, the bias voltage was varied from −30 to +30 V (Fig. 2). An image clearly indicated the bacteria at a bias of −30 V using a 4 kV EB with current of 250 pA, its SNR is 33.6 dB (Fig. 2A). The image contrast and SNR gradually decreased when the bias increased from −30 to −15 V (Fig. 2B). At 0 V bias, no image was obtained because of the minimum SNR (Fig. 2C). Above 0 V, the contrast and SNR gradually increased, which improved the image (Fig. 2D and E). However, the image SNR at +30 V bias was lower than that at −30 V bias. Image contrast and SNR depend on the output signal amplitude (Fig. 2A). While the image completely disappeared at 0 V bias of 250 pA EB current (Fig. 2C), the bacteria were detectable when irradiated using a 2.4 nA EB (Fig. 2F).

Because intact bacteria in water were observed without radiation damage, their movement was detectable by multi-scanning of the same specimens through this method. In the first scanned image, many rod shape bacteria were dispersed in the water (Supplementary Fig. 3A). A minute later, the same specimens examined under the same conditions exhibited slight differences (Supplementary Fig. 3B), suggesting bacterial movement. This movement was confirmed at the expanded images (Supplementary Fig. 3C, E vs. 3D, F, white and black arrows). However, these displacements were small because the bacteria would be bound to the SiN film.

The intact bacteria in water were further analysed at high magnification (Fig. 3). Fig. 3A shows a 10,000× magnification FTE image of the bacteria at −30 V bias voltage. The contrast of the bacterial contours undulated slightly, which is typical of bacterial inner structure. For detailed investigation, the left bottom area of Fig. 3A was expanded and contrast-enhanced (Fig. 3B). Thin fibres were detected around the bacterial body (Fig. 3B, red arrows), which were attributed to flagella. Bacterium flagella are very narrow (12–25 nm) [30,31] and generally require negative staining or metal coating to be observed [29,31]. In contrast, our FTE

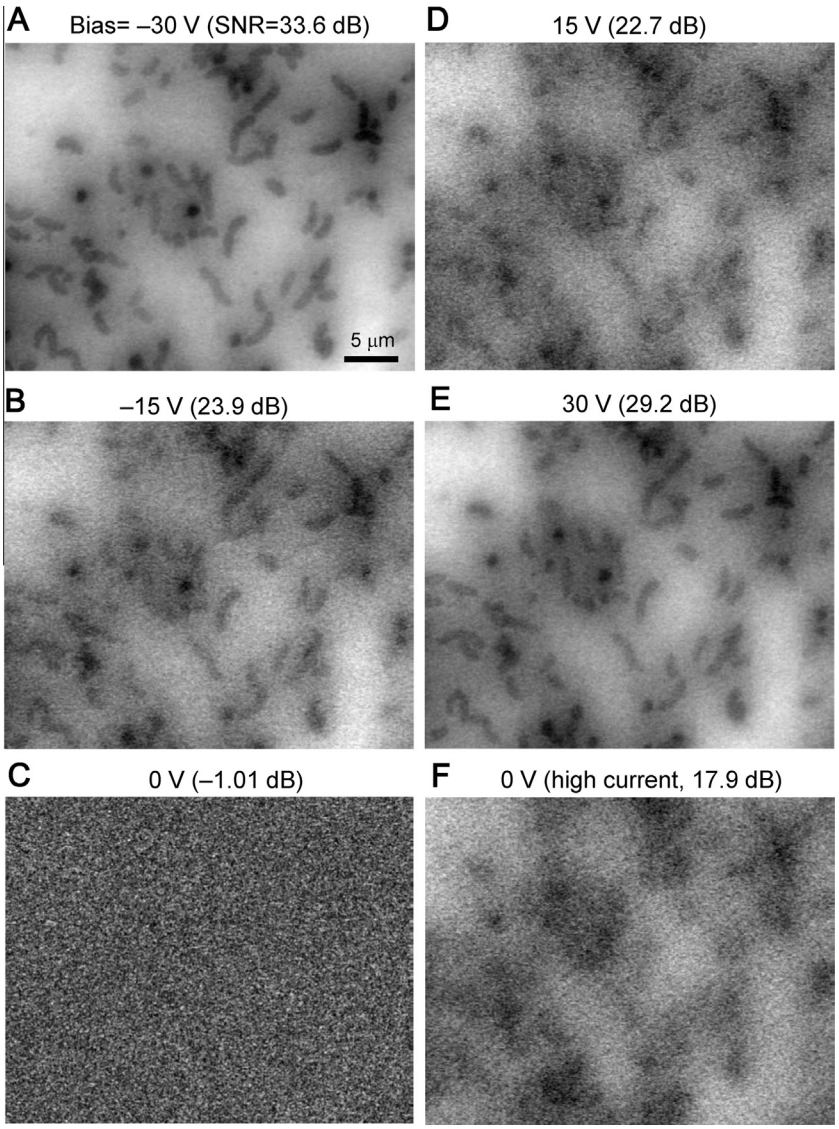

Fig. 2. Images of unstained bacteria in water at various bias voltages. (A) Image presenting clear black contrast at a magnification of 2000× and bias voltage of −30 V under EB irradiation at an acceleration voltage of 4 kV and 250 pA. The image SNR is 33.6 dB. The scale bar represents 5 μm. (B) Image showing a decrease in the black contrast at a bias voltage of −15 V. (C) Image obtained at 0 V bias showing the absence of contrast. (D) At a bias voltage of 15 V, the bacteria gradually emerged in black contrast. (E) At a bias voltage of 30 V, the contrast was clearer. (F) At a bias voltage of 0 V and high EB current of 2.4 nA, images became barely visible.

method enables their detection in water without staining. A pseudo-colour map of these specimens was created to investigate the bacterial inner structure (Fig. 3C and D). These colour maps exhibited a high-density region in the upper portion of the bacteria, suggesting the presence of the nucleoid. The averaged lineout across the bacteria edge is shown Fig. 3E. The spatial resolution of the high-sensitive FTE system using thermionic SEM is 41 nm (Fig. 3F), which is defined as the width over which the normalised intensity decreases from 0.75 to 0.25 in the lineout [32]. The spatial resolution of 41 nm is considerably higher than the previous FTE system [19].

Finally, an intact rod-shaped 200–350 nm long baculovirus with a diameter ranging between 60 and 100 nm [33–35] was observed in water to further assess the performance of the new FTE system (Fig. 4). The unstained specimen in water displayed small rod-shaped particles with black contrast at 10,000× magnification and −30 V bias voltage (Fig. 4A). An expanded image of the baculovirus clearly showed the rod-shaped structure (Fig. 4B). Furthermore, the virion presented a small grain in the lower right side (Fig. 4B, black arrow) consisting with its envelope [33]. A pseudo-colour map of this virion provided a clearer image of the envelope (Fig. 4C).

4. Discussion

Examining unstained and unfixed bacteria and virus in water at high contrast without incurring radiation damage is difficult. Unstained biological specimens observed by SEM in water using atmospheric sample holders show very low contrast because they weakly interact with the EB and display densities similar to that of water. Furthermore, intact biological specimens suffer serious EB-induced radiation damage [16–18].

Here, a high-contrast and non-destructive method was developed to meet this challenge. In this high-sensitivity FTE system, the biological specimens were placed in the space between two SiN films. The W–Ni coated SiN film was irradiated with the chopped EB at an acceleration voltage of 4 kV. The irradiated

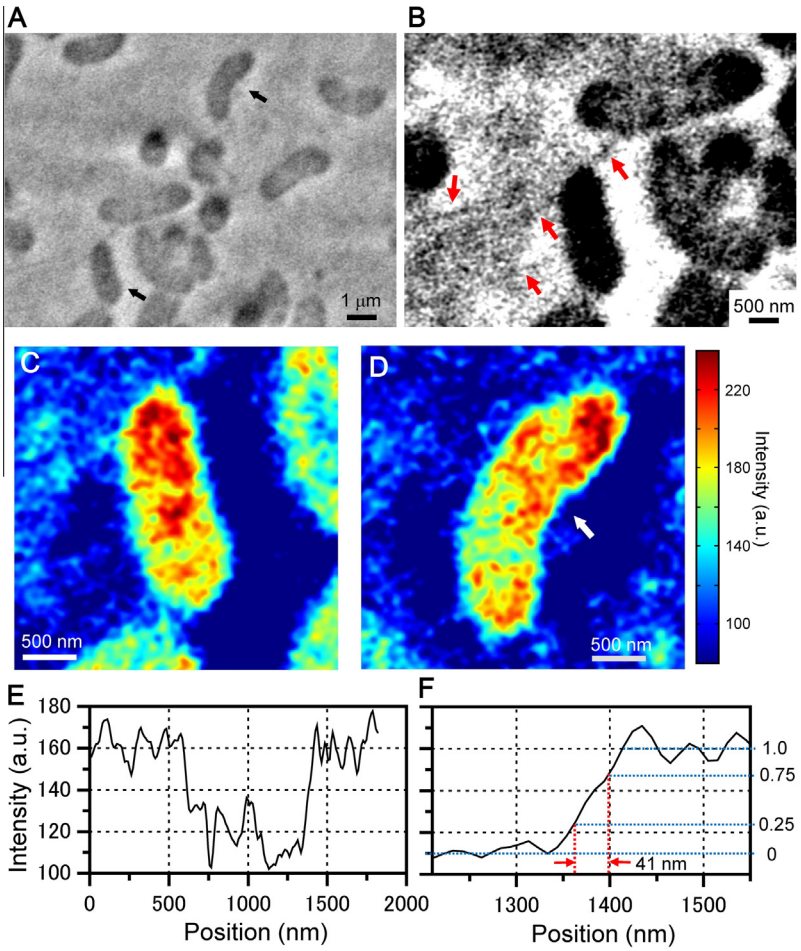

Fig. 3. High magnification image of unstained and unfixed bacteria in water obtained using the FTE system. (A) FTE image in water at 10,000× magnification under EB irradiation at an acceleration voltage of 4 kV and a frequency of 30 kHz. The image was filtered using a 2D GF (7 × 7 pixel, $\sigma = 2$) after background subtraction. The unstained bacteria exhibited a weak black contrast. (B) Expansion of the bottom left area in (A) showing further contrast enhancement. Red arrows indicate flagella. (C, D) Expanded pseudo-colour images of bacteria indicated by black arrows in (A). These images were using the 2D GF (11 × 11 pixel, $\sigma = 3$) after intensity inversion. The area in red indicates a low-intensity region corresponding to a high-density area. The high-density region was detected in the upper portion of the bacteria. (E) An averaged lineout across the bacteria edge in (D) white arrow, which averaged 15 lines. (F) A lineout of the right side edge in the bacteria. Spatial resolution of the high-sensitive FTE method using thermionic SEM is 41 nm. That is defined as the width over which the normalised intensity decreases from 0.75 to 0.25 in the lineout. Scale bars represent 1 μm in (A) and 500 nm in (B)–(D). (For interpretation of the references to colour in this figure legend, the reader is referred to the web version of this article.)

electrons were almost absorbed in the 20 nm-thick W layer [19] because of the high-density metal (19.3 g/cm^3), facilitating the non-destructive observation of biological specimens. The chopped EB gave rise to an electric potential oscillation in the SiN film W layer, which was transmitted to the measurement terminal through the biological samples in the water layer (Fig. 1). Furthermore, the detection signal was highly enhanced when voltage was applied to the metal layer. More importantly, a −30 V bias voltage improved the output signal hundredfold (Supplementary Fig. 1). Consequently, unlike the unbiased system, the bias voltage increased the spatial resolution and S/N ratio (Figs 2 and 3). Therefore, the new system enables the observation of bacteria and viruses in water at higher resolution (Figs. 3 and 4). The signal enhancement may stem from the effect of the bias voltage-induced parallel electric field on the water dipole (Supplementary Fig. 4). At 0 V bias, water dipoles adopt a random orientation (Supplementary Fig. 4A). Furthermore, at a negative bias voltage, these dipoles are slightly oriented according to the parallel electric field originating from the metal layer (Supplementary Fig. 4B). Therefore, the chopped EB signal may be easily transmitted to the measurement terminal by the pre-oriented dipoles (Supplementary Fig. 4C and D). The motion produced by the nonuniform electric field of dielectrophoresis may be helpful in the theoretical analysis of FTE [36,37]. This proposed signal enhancement mechanism will be further investigated experimentally and/or theoretically based on dielectrophoresis system.

The FTE method was sufficient for the detailed observation of the bacterial structure (Fig. 3). However, the spatial resolution of 41 nm was unsatisfactory for virus analysis (Fig. 4). Studies are currently underway to improve this spatial resolution. To exceed a resolution of 10 nm, a system will be developed using high-resolution field-emission SEM. The future high-resolution FTE system is expected to enable the imaging of unstained and intact macromolecular and membrane proteins.

In conclusion, high-resolution imaging of intact biological specimens in water was conducted using a high-sensitivity SEM-based FTE system. The resulting images clearly exhibited unstained and unfixed bacteria and viruses; its spatial resolution is 41 nm. This method offers very low radiation damage to the sample. Furthermore, it can be used for diverse liquid samples across a broad range of scientific fields, such as nanoparticles, organic materials and catalytic materials.

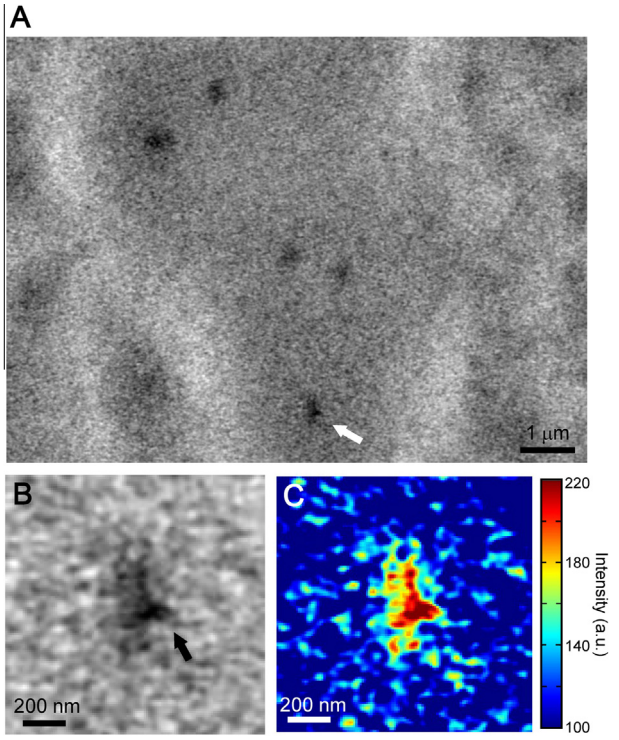

Fig. 4. High-resolution image of unstained baculoviruses in water. (A) FTE image at 10,000× magnification under EB irradiation at an acceleration voltage of 4 kV and a frequency of 30 kHz. The image was filtered using the 2D GF (7 × 7 pixel, $\sigma = 1$) after background subtraction. Small rod-shaped particles correspond to viruses. (B) Expansion of the area indicated by the white arrow in (A) with further contrast enhancement. The image was filtered using the 2D GF (7 × 7 pixel, $\sigma = 1.5$). The virion showed a small grain in the lower right side (black arrow). (C) Expanded pseudo-colour image of (B) after intensity inversion. The colour map image clearly displayed rod-shaped structures containing a small grain. Scale bars represent 1 μm in (A) and 200 nm in (B) and (C). (For interpretation of the references to colour in this figure legend, the reader is referred to the web version of this article.)

Acknowledgments

This study was supported by a KAKENHI Grant-in-Aid for Scientific Research (B) and for the Challenging Exploratory Research of the Japan Society for the Promotion of Science.

Appendix A. Supplementary data

Supplementary data associated with this article can be found, in the online version, at http://dx.doi.org/10.1016/j.bbrc.2014.07.062.

References

[1] V. Lucic, A. Rigort, W. Baumeister, Cryo-electron tomography: the challenge of doing structural biology in situ, J. Cell Biol. 202 (2013) 407–419.
[2] A. Sali, R. Glaeser, T. Earnest, et al., From words to literature in structural proteomics, Nature 422 (2003) 216–225.
[3] A. Leis, B. Rockel, L. Andrees, et al., Visualizing cells at the nanoscale, Trends Biochem. Sci. 34 (2009) 60–70.
[4] Y.M. Wu, C.H. Wang, J.W. Chang, et al., Zernike phase contrast cryo-electron microscopy reveals 100 kDa component in a protein complex, J. Phys. D Appl. Phys. 46 (2013) 494008.
[5] Y. Inayoshi, H. Minoda, Y. Arai, et al., Direct observation of biological molecules in liquid by environmental phase-plate transmission electron microscopy, Micron 43 (2012) 1091–1098.
[6] J. Frank, Single-particle imaging of macromolecules by cryo-electron microscopy, Annu. Rev. Biophys. Biomol. Struct. 31 (2002) 303–319.
[7] E.J. Wood, R.J. Seviour, A.B.M. Siddique, et al., Spherical body formation in the spirochaete *Brachyspira hyodysenteriae*, FEMS Microbiol. Lett. 259 (2006) 14–19.
[8] N. Minoura, S. Aiba, M. Higuchi, et al., Attachment and growth of fibroblast cells on silk fibroin, Biochem. Biophys. Res. Commun. 208 (1995) 511–516.
[9] J.G. Duckett, R. Ligrone, The formation of catenate foliar gemmae and the origin of oil bodies in the liverwort *Odontoschisma denudatum* (Mart.) dum (Jungermanniales): a light and electron microscope study, Ann. Bot. 76 (1995) 405–419.
[10] P.M. Motta, S. Makabe, T. Naguro, et al., Oocyte follicle cells association during development of human ovarian follicle. A study by high resolution scanning and transmission electron microscopy, Arch. Histol. Cytol. 57 (1994) 369–394.
[11] R. Lamed, J. Naimark, E. Morgenstern, et al., Scanning electron microscopic delineation of bacterial surface topology using cationized ferritin, J. Microbiol. Methods 7 (1987) 233–240.
[12] S.R. Richards, R.J. Turner, A comparative study of techniques for the examination of biofilms by scanning electron microscopy, Water Res. 18 (1984) 767–773.
[13] J.M. Rowe, J.R. Dunlap, C.J. Gobler, et al., Isolation of a non-phage-like lytic virus infecting *Aureococcus anophagefferens*, J. Phycol. 44 (2008) 71–76.
[14] S. Thiberge, A. Nechushtan, D. Sprinzak, et al., Scanning electron microscopy of cells and tissues under fully hydrated conditions, Proc. Natl. Acad. Sci. U.S.A. 101 (2004) 3346–3351.
[15] N. de Jonge, D.B. Peckys, G.J. Kremers, et al., Electron microscopy of whole cells in liquid with nanometer resolution, Proc. Natl. Acad. Sci. U.S.A. 106 (2009) 2159–2164.
[16] R. Henderson, R.M. Glaeser, Quantitative analysis of image contrast in electron micrographs of beam-sensitive crystals, Ultramicroscopy 16 (1985) 139–150.
[17] R.M. Glaeser, Limitations to significant information in biological electron microscopy as a result of radiation damage, J. Ultrastruct. Res. 36 (1971) 466–482.
[18] R.F. Egerton, P. Li, M. Malac, Radiation damage in the TEM and SEM, Micron 35 (2004) 399–409.
[19] T. Ogura, Direct observation of unstained biological specimens in water by the frequency transmission electric-field method using SEM, PLoS One 9 (2014) e92780.
[20] K. Boone, A.M. Lewis, D.S. Holder, Imaging of cortical spreading depression by EIT: implications for localization of elieptic foci, Physiol. Meas. 15 (1994) A189–A198.
[21] A. McEwan, G. Cusick, D.S. Holder, A review of errors in multi-frequency EIT instrumentation, Physiol. Meas. 28 (2007) S197–S215.
[22] G. Boverman, D. Isaacson, G.J. Saulnier, et al., Methods for compensating for variable electrode contact in EIT, IEEE Trans. Biomed. Eng. 56 (2009) 2762–2772.
[23] R. Kulkarni, T.J. Kao, G. Boverman, et al., A two-layered forward model of tissue for electrical impedance tomography, Physiol. Meas. 30 (2009) S19–S34.
[24] D.T. Nguyen, C. Jin, A. Thiagalingam, et al., A review on electrical impedance tomography for pulmonary perfusion imaging, Physiol. Meas. 33 (2012) 695–706.
[25] E. Brandis, A. Rosencwaig, Thermal-wave microscopy with electron beams, Appl. Phys. Lett. 37 (1980) 98–100.
[26] G.S. Cargill, Ultrasonic imaging in scanning electron microscopy, Nature 286 (1980) 691–693.
[27] T.G. Lilburn, C.E. Haith, R.C. Prince, et al., Pleiotropic effects of *pufX* gene deletion on the structure and function of the photosynthetic apparatus of *Rhodobacter capsulatus*, Biochim. Biophys. Acta 1100 (1992) 160–170.
[28] F. Oling, E.J. Boekema, I.O. de Zarate, et al., Two-dimensional crystals of LH2 light-harvesting complexes from *Ectothiorhodospira sp.* and *Rhodobacter capsulatus* investigated by electron microscopy, Biochim. Biophys. Acta 1273 (1996) 44–50.
[29] K.J. Shelswell, T.A. Taylor, J.T. Beatty, Photoresponsive flagellum-independent motility of the purple phototrophic bacterium *Rhodobacter capsulatus*, J. Bacteriol. 187 (2005) 5040–5043.
[30] K. Yonekura, S. Maki-Yonekura, K. Namba, Complete atomic model of the bacterial flagellar filament by electron cryomicroscopy, Nature 424 (2003) 643–650.
[31] S. Cohen-Krausz, S. Trachtenberg, The flagellar filament structure of the extreme acidothermophile *Sulfolobus shibatae* B12 suggests that archaeabacterial flagella have a unique and common symmetry and design, J. Mol. Biol. 375 (2008) 1113–1124.
[32] L. Reimer, Scanning electron microscopy: Physics of image formation and microanalysis, second ed., Springer, Heidelberg, 1998.
[33] G.F. Rohrmann, Baculovirus structural proteins, J. Gen. Virol. 73 (1992) 749–761.
[34] G.H. Bergold, The molecular structure of some insect virus inclusion bodies, J. Ultrastruct. Res. 8 (1963) 360–378.
[35] N.D. van Loo, E. Fortunati, E. Ehlert, et al., Baculovirus infection of nondividing mammalian cells: mechanisms of entry and nuclear transport of capsids, J. Virol. 75 (2001) 961–970.
[36] H.A. Pohl, The motion and precipitation of suspensoids in divergent electric fields, J. Appl. Phys. 22 (1951) 869–871.
[37] H.A. Pohl, J.S. Crane, Dielectrophoresis of cells, Biophys. J. 11 (1971) 711–727.